Journal of Materials Chemistry

Cite this: J. Mater. Chem., 2012, 22, 15819

www.rsc.org/materials

PAPER

Synthesis of ternary transition metal fluorides Li_3MF_6 *via* a sol–gel route as candidates for cathode materials in lithium-ion batteries†

Julia Kohl,[a] Dennis Wiedemann,[a] Suliman Nakhal,[a] Patrick Bottke,[b] Noel Ferro,[c] Thomas Bredow,[c] Erhard Kemnitz,[d] Martin Wilkening,[b] Paul Heitjans[e] and Martin Lerch*[a]

Received 5th April 2012, Accepted 8th June 2012
DOI: 10.1039/c2jm32133e

A sol–gel route for ternary lithium fluorides of transition metals (M) is presented allowing the synthesis of Li_3MF_6-type and Li_2MF_5-type compounds. It is based on a fluorolytic process using transition metal acetylacetonates as precursors. The domain size of the obtained powders can be controlled by modifying the conditions of synthesis. ^{6}Li and ^{7}Li magic angle spinning (MAS) nuclear magnetic resonance (NMR) spectroscopy is used to study local environments of the Li ions in orthorhombic and monoclinic Li_3VF_6 as well as Li_2MnF_5. The number of magnetically inequivalent Li sites found by MAS NMR is in agreement with the respective crystal structure of the compounds studied. Quantum chemical calculations show that all materials have high de-lithiation energies making them suitable candidates to be used as high-voltage battery cathode materials.

Introduction

The search for new cathode materials as part of lithium-ion batteries is an important objective today.[1–5] Currently, oxides such as $LiCoO_2$, layered Li–Mn-spinels as well as olivine-type structures such as $LiFePO_4$ are in the focus of interest.[6,7] Modern cathode materials need to fulfil many different requirements. Promising compounds are supposed to exhibit high concentrations of lithium in order to achieve high energy densities and capacities. In addition, besides a good electronic conductivity, sufficiently high lithium-ion diffusivity is one of the prerequisites for facile lithium insertion and removal. Finally, chemical and thermal stability of the components directly affect the cyclability of the lithium-ion battery and thus its lifetime.

Until recently, various oxide materials have been in the focus of research.[6,7] Interestingly, theoretical calculations indicate a large increase of the redox potential by substituting fluorine for oxygen.[8] Consequently, ternary lithium fluorides are increasingly considered for advanced electrochemical characterization. In particular, the Li_3MF_6 (M = transition metal) family exhibits high lithium contents combined with variable oxidation numbers. Recently, Gonzalo *et al.* reported Li_3FeF_6 to be a promising cathode material for lithium-ion batteries.[9] Furthermore, the electrochemical properties of Li_3VF_6 prepared by microwave synthesis have been studied quite recently.[10a] In addition, Li_3VF_6 is also in the focus of a low-temperature precipitation route in aqueous solution using alcohols recently reported by Basa *et al.*[10b] The relatively low capacity of the compounds is assumed to increase with decreasing particle size. Therefore, the preparation of Li_3MF_6 phases with particle sizes less than 50 nm, as successfully shown by Basa *et al.*,[10b] is of great interest to improve the associated electrochemical performance. The compounds Li_3MF_6 (M = V, Cr, Fe) are known to exist in two polymorphs. Whereas the monoclinic form (space group $C2/c$) crystallizes isotypically with β-Li_3AlF_6, the orthorhombic modification crystallizes with the space group $Pna2_1$ being identical to that of the corresponding α-form of Li_3AlF_6. The two polymorphs are structurally related to the cryolite type.[11,12]

Usually, the monoclinic polymorph is obtained by slow cooling down of a stoichiometric mixture of the binary fluorides to room temperature, while the orthorhombic form can only be prepared by quenching the samples from an elevated ($T > 600$ K) to ambient temperature. Due to the poor electronic conductivity of transition metal fluorides the design of particle morphology is of great importance for potential electrochemical applications. Since ternary transition metal fluorides are usually synthesized by solid-state reactions at high temperatures and/or high pressures, the obtained particles show diameters in the micrometer

[a]Technische Universität Berlin, Department of Chemistry, Straße des 17. Juni 135, 10623 Berlin, Germany. E-mail: martin.lerch@tu-berlin.de; Fax: +49 030 314 22740; Tel: +49 030 314 22603
[b]Technische Universität Graz, Institut für Chemische Technologie von Materialien, Stremayrgasse 9, 8010 Graz, Austria. E-mail: wilkening@tugraz.at; Fax: +43 316 873 32332; Tel: +43 316 873 32330
[c]Universität Bonn, Mulliken Center for Theoretical Chemistry, Department of Physical and Theoretical Chemistry, Beringstr. 4, 53115 Bonn, Germany. E-mail: bredow@thch.uni-bonn.de; Fax: +49 0228 73 9064; Tel: +49 0228 73 3839
[d]Humboldt-Universität zu Berlin, Department of Chemistry, Brook-Taylor-Straße 2, 12489 Berlin, Germany. E-mail: erhard.kemnitz@chemie.hu-berlin.de; Fax: +49 030 2093 7277; Tel: +49 030 2093 7555
[e]Leibnitz Universität Hannover, Insitute of Phyiscal Chemistry and Electrochemistry, Callinstr. 3 – 3a, 30167 Hannover, Germany. E-mail: heitjans@pci.uni-hannover.de; Tel: +49 511 762 3187

† CCDC 868968. For crystallographic data in CIF or other electronic format see DOI: 10.1039/c2jm32133e

range. Generally, nm-sized particles can be easily prepared by high-energy ball milling of the coarse grained materials.[13–15] Besides activation, mechanochemistry has also successfully been used for the synthesis of a variety of materials from precursors at room temperature including oxides and fluorides.[16–18] However, in contrast to such a top-down approach, the preparation of nanostructured particles by precipitation from aqueous solution is much more beneficial when the shape and surface morphology of the crystallites have also to be controlled. By following such a route, the corresponding salts, for example nitrates or oxides, are reacted with hydrofluoric acid and subsequent dehydration is carried out by annealing at elevated temperatures. In general, solution-based syntheses offer many advantages. For instance, low temperatures and good mixing of the precursors allow the preparation of highly homogeneous compounds with a large surface area. In contrast to aqueous routes, syntheses carried out in organic solvents provide a large range of different media with versatile characteristics. When HF is dissolved directly in an organic solvent, competing reactions between HF and H_2O with the transition metal can be eliminated. When, for example, alcoholates or acetylacetonates are used as starting materials the corresponding alcohols or acetylacetone is formed which can easily be removed under vacuum. Moreover, due to very fast crystallization materials consisting of very small particle diameters (low nm-range) can be obtained.

To our knowledge only few reports can be found in the literature which report on the synthesis of ternary fluorides from these starting materials. Kemnitz *et al.* presented the synthesis of aluminum and magnesium fluorides with high surface areas by a fluorolytic sol–gel process.[19,20] These studies illustrate the synthetic potential of organic hydrogen fluoride solutions. Aluminum compounds crystallizing in the cryolite or elpasolite type were prepared from the corresponding alcoholates. For example, Li_3AlF_6 can be obtained *via* the reaction of LiO*t*Bu and Al(O*i*Pr)$_3$ with HF in isopropanol.[21] This method allows one to work under water-free conditions. Concerning transition metal fluorides only acetylacetonates, acetates and, in the case of iron, alcoholates are obtainable as starting materials. The aim of our present work is to develop a nonaqueous sol–gel route for the preparation of Li_3MF_6 compounds (M = V, Cr, Fe, Mn, Co) and to elucidate the possibilities of controlling the size of the particles synthesized.

Experimental section

X-ray powder diffraction

X-ray powder diffraction experiments were performed using a PANalytical X'Pert PRO MPD diffractometer (CuK_α-radiation, 2θ range 5 to 120°, Bragg–Brentano (θ–θ) geometry) with PIXcel detector (Si–Li-semiconductor with 255 measuring channels). All samples were prepared on small Si-cavity mounts.

X-ray fluorescence

For X-ray fluorescence analysis, a PANalytical Axios PW4400/24 X-ray fluorescence spectrometer with an Rh-tube and wavelength-dispersive detection was used. Depending on the analyzed elements a LiF single crystal (crystallographic orientation (220) and (200)), a Ge single crystal (orientation (111)), a PE single crystal (orientation (002)) and a PX1 multi-layer monochromator were used together with an Si(Li) scintillation detector.

NMR

Liquid-phase ^{1}H, ^{13}C, ^{51}V, and ^{19}F NMR spectra were recorded on a Bruker Avance 200 and a Bruker Avance 400 NMR spectrometer. TMS, $CFCl_3$ and $VOCl_3$ served as references. Solid-state high-resolution, *i.e.*, magic angle spinning (MAS), ^{6}Li and ^{7}Li NMR spectra were acquired using Avance III NMR (Bruker BioSpin) spectrometers connected to cryomagnets with nominal fields of 7 T and 14.1 T. This results in ^{6}Li resonance frequencies of 44 and 88 MHz and ^{7}Li resonance frequencies of 117 and 233 MHz, respectively. We used a standard (double-resonance) 2.5 mm-probe (Bruker) which can be operated at spinning speeds of up to 30 kHz. Additionally, some ^{6}Li MAS NMR spectra were recorded with an Avance NMR spectrometer being connected to a cryomagnet with a nominal magnetic field of 17.6 T. The spectrometer can be used in combination with an MAS NMR probe allowing a maximum spinning speed of 15 kHz. The Li MAS NMR spectra shown were referenced to LiCl (aq). They were recorded using a single excitation pulse and recycling delays of up to several seconds. ^{6}Li and ^{7}Li NMR spin–lattice relaxation times T_1 of the paramagnetic Li_3MF_6 and Li_2MnF_5 samples were measured with a conventional saturation recovery experiment using up to 12 different delay times. As expected, the T_1 values associated with the paramagnetic shifts do not exceed 100 ms. Preliminary 2D exchange MAS NMR spectra of Li_2MnF_5 were recorded using a conventional NOESY pulse sequence. Time domains of 512 data points in both *f*1 and *f*2 directions were used. Processing of the data was carried out using TopSpin 3.1 software (Bruker) and Mnova7 (Mestrelab research).

FTIR

FTIR spectra were measured on a Varian 640IR FTIR spectrometer equipped with a Pike GladiATR device for measurements in attenuated total reflectance mode. FTIR spectra of KBr pellets and CsI pellets were measured with a Nicolet Series II Magna-IR System 750 FTIR spectrometer in transmission mode.

Elemental analysis

The carbon and hydrogen contents were determined by combustion analysis (Thermo Finnigan FlashEA 1112 NC analyzer), the oxygen contents using a LECO EF-TC 300 N_2/O_2 analyzer (hot gas extraction).

Materials and methods

V(acac)$_3$ (ABCR), Fe(acac)$_3$, Cr(acac)$_3$, Mn(acac)$_3$, Mn(OAc)$_3\cdot 2H_2O$, Co(acac)$_3$ and LiO*t*Bu (Sigma-Aldrich) were used as received. Solutions of HF in ethanol, THF and Et_2O were prepared by feeding gaseous HF into the solvent under cooling. The solvents were dried according to standard literature procedures. All reactions were carried out using standard Schlenk techniques. Reagents and samples were stored in an Ar-filled glove box.

General synthesis

Precursor synthesis, Li_3VF_6 as example: 1 g (2.87×10^{-3} mol) of $V(acac)_3$ and 0.6895 g (8.61×10^{-3} mol) of Li*O*t*Bu (Li : V = 3 : 1) were weighed into a Schlenk tube and suspended in 20 ml of absolute ethanol at room temperature for 30 min. To the resultant suspension 8.40 ml of a 10.25 M HF–EtOH solution was added leading to a green solution (V : HF = 1 : 30). Alternatively, a 6.89 M HF–Et_2O or a 10.68 M HF–THF solution was used. The solution was stirred for 2 h at room temperature. Afterwards, the solvent was removed under vacuum and the resultant fine green powder was dried at 80 °C for 2 h.

Synthesis of the Li_3MF_6 samples: all syntheses were carried out in sealed copper or monel capsules under nitrogen atmosphere. 100 to 200 mg of the precursor were filled into a one-side sealed capsule. If not stated otherwise, all samples were slowly cooled down to room temperature. In Table 1, the synthesis conditions of the fluorides prepared are listed.

$V(acac)_2(CH_3CN)_2BF_4$: a saturated solution of the Li_3VF_6 precursor was prepared in 10 ml of absolute CH_3CN and stirred overnight at 50 °C. The resulting green-brown solution was filled in small glass tubes. These glass tubes were positioned in a Schlenk tube filled with 20 ml of absolute Et_2O. After approximately 20 days dark red crystals were formed.

Results and discussion

Monoclinic and orthorhombic Li_3VF_6

As described in the Experimental section, Li_3VF_6 can be prepared by a two-step synthesis. During the first step the so-called precursor is synthesized. Li*O*t*Bu and $V(acac)_3$ react with hydrogen fluoride in a dry solvent (Li : V : HF = 3 : 1 : 30). After evaporating the solvent and drying, the obtained Li_3VF_6 precursor is calcined at 300 to 800 °C to form Li_3VF_6. The precursor can be described as a fine, green and mainly X-ray amorphous powder. The corresponding X-ray powder pattern shows that the precursor also contains poorly crystalline LiF and Li_2SiF_6. The latter phase results from the reaction of HF with the glassware used. However, Li_2SiF_6 does not affect the subsequent reactions because it decomposes into LiF and SiF_4 at temperatures above 250 °C.[22] As determined by X-ray fluorescence analysis, all samples contain approximately 3 to 4.5% Si. Interestingly, small amounts of Li_2SiF_6 were also formed when the synthesis was carried out in a glass Schlenk tube equipped with a closed PTFE insert inside (Fig. 1b and c). This insert was opened after synthesis for removing the solvent under vacuum.

Table 1 Synthesis conditions for the Li_3MF_6 compounds (orth. = orthorhombic and mon. = monoclinic)

Compound	Dwell time	Temperature	Further conditions
Li_3VF_6, orth.	2 h	700 °C	Quenching to room temperature after 2 h
Li_3VF_6, mon.	4 h	150 to 600 °C	
Li_3FeF_6, orth.	2 h	800 °C	Quenching to room temperature after 1 h
Li_3FeF_6, mon.	4 h	400 to 600 °C	
Li_3CrF_6, mon.	4 h	500 °C	
Li_2MnF_5	4 h	400 °C	30% Li_2MnF_5

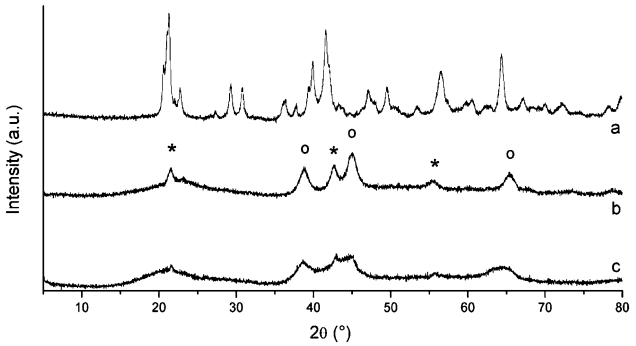

Fig. 1 X-ray powder diffraction patterns of different Li_3VF_6 precursors: (a) precursor decomposition at 300 °C (Li_2SiF_6 has been completely decomposed), (b) synthesis in glassware, (c) synthesis with PTFE insert (o = LiF, * = Li_2SiF_6).

Surprisingly, remaining HF seems to react immediately with the glassware in which the PTFE tube is inserted. Note that from X-ray diffraction no information on the nature of the vanadium species can be obtained.

Li_3VF_6, which was prepared by decomposition of the precursor, was also analyzed by X-ray powder diffraction. Heating to 300 °C leads to the formation of Li_3VF_6. Li_2SiF_6 seems to be completely decomposed (see also Fig. 1a). From the XRD patterns there are only vague indications of very small amounts of remaining LiF not reacted with vanadium species of the precursor. When the samples were cooled down to room temperature slowly, monoclinic Li_3VF_6 was observed. Heating the precursor to 700 °C and quenching the sample to room temperature results in the formation of orthorhombic Li_3VF_6 as described in the literature (see Fig. 2). Both polymorphs were obtained with more than 98% purity. Elemental analysis resulted in a residual carbon content of approximately 2%.

Besides the successful preparation of highly pure α-Li_3VF_6 and β-Li_3VF_6, it is also possible to modify the domain size of the samples prepared. For example, this can easily be achieved by

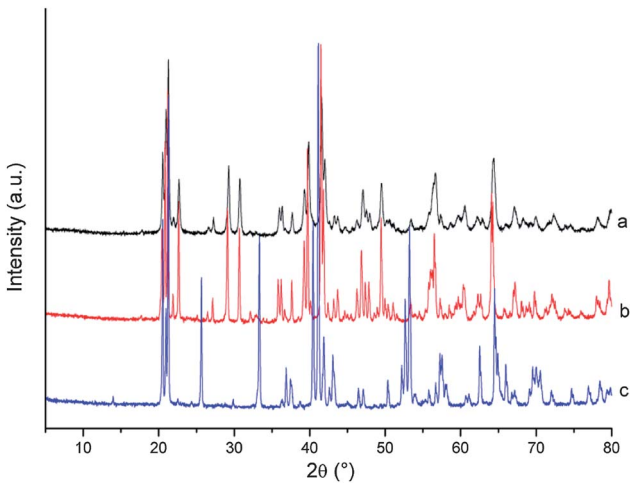

Fig. 2 X-ray powder diffraction patterns of monoclinic β-Li_3VF_6 synthesized at (a) 300 °C and (b) 600 °C. (c) Corresponding X-ray powder pattern of orthorhombic α-Li_3VF_6 which has been synthesized at 700 °C and by subsequent quenching to room temperature.

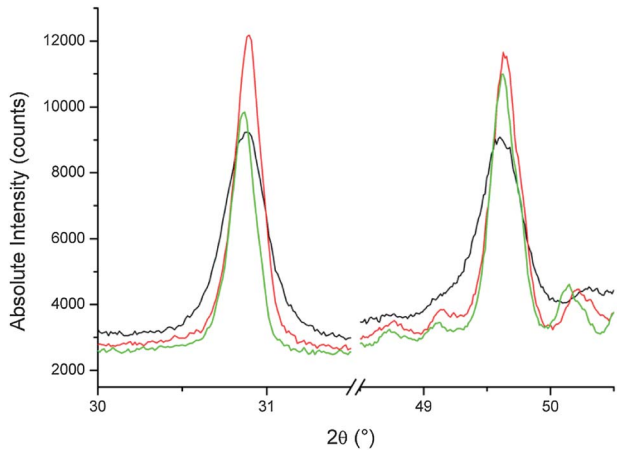

Fig. 3 Temperature-dependent broadening of the reflections at $2\theta = 30.72°$ and $2\theta = 49.45°$ of monoclinic Li_3VF_6 (400 °C (black), 500 °C (red), 600 °C (green)). All samples were slowly cooled down to room temperature.

varying the synthesis temperature as presented in the following. The precursors were heated for 4 h at 400, 500 and 600 °C, respectively. As shown in Fig. 3, the full width at half maximum of the diffraction reflections decreases with increasing temperature. The domain sizes were calculated by methods based on the Scherrer formula.[26] The results are depicted in Table 2. Here, the domain size can be varied from approximately 30 to 200 nm which is the range of interest for electrochemical applications. In general, the domain size increases with increasing temperature. For different solvents the absolute values as well as the temperature dependence of the sizes differs significantly. The reason for this is unclear. First investigations of the samples by means of standard SEM resulted in an average particle size of ~200 nm for the samples synthesized at 400 °C.

Typical ^{6}Li MAS NMR spectra of polycrystalline α-Li_3VF_6 and β-Li_3VF_6 are shown in Fig. 4. In agreement with the crystal structure of the orthorhombic modification the NMR spectrum of α-Li_3VF_6 reveals three distinct lines which can be attributed to the Li positions Li(1), Li(2), and Li(3) as shown recently by some of us.[23] The NMR shifts result from the Fermi-contact interaction which is related to the extent of electron spin density transferred from the V^{3+} t_{2g} orbital to the 2s orbital Li ion. In ref. 23 the assignment of the NMR lines presented has been based on (i) results from temperature-variable 1D and 2D exchange NMR experiments, (ii) the considerations of different mechanisms to transfer electron spin density, and (iii) the connectivities of the VF_6 and LiF_6 polyhedra in α-Li_3VF_6. Note that with increasing temperature the lines first broaden and finally coalesce because of Li ion exchange taking place on the timescale determined by the distance of the NMR lines (see Fig. 1 in ref. 23). The beginning of this process can already be recognized when the spectrum shown in Fig. 4c is considered. At lower temperatures, note that NMR spectra down to 277 K were recorded, no additional lines show up indicating that the three lines observed are not affected by any coalescence phenomena occurring at lower temperatures. The three lines detected show approximately the same intensity which is expected from the crystal structure where the three crystallographically inequivalent Li sites, residing on the same Wyckoff position 4a, are fully occupied.

Interestingly, the individual paramagnetic NMR shifts δ depend on temperature. A linear relationship between δ and $1/T$ is expected for the Curie–Weiss behavior quantifying the dependence of the magnetic susceptibility on temperature. The larger the paramagnetic shift the steeper the slope of the corresponding δ ($1/T$) line: see, *e.g.*, the recent study by Spencer *et al.*[24] This effect can be clearly seen in Fig. 4d–f showing the ^{6}Li MAS NMR spectra of the monoclinic counterpart of Li_3VF_6. Up to 353 K no coalescence of the NMR lines is observed.

In β-Li_3VF_6 the Li ions occupy five crystallographically inequivalent sites whereby Li(2), Li(3), Li(4) and Li(5) reside on the Wyckoff position 8f and Li(1) on 4e. Since all the sites are fully occupied one might ascribe the NMR signal with the lowest intensity and the largest paramagnetic shift (76 ppm at 333 K) to the Li(1) ions. The asymmetric shape of this NMR peak might indicate that the signal is composed of more than one line, *i.e.*, the ions residing on the position 4e are crystallographically equivalent but not magnetically so. The assignment of the other NMR peaks, which do not differ in intensity as expected from the crystal structure, requires mixing time dependent 2D exchange NMR experiments and a careful analysis of the relevant transfer mechanisms of electron spin density. Such a study is beyond the scope of the present contribution and will be published elsewhere together with an investigation of the Li hopping processes taking place in β-Li_3VF_6. First results were shown in ref. 25. Comparing the 1D ^{6}Li MAS NMR spectra shown in ref. 23 with those obtained from α-Li_3VF_6 and presented in Fig. 4, it is already evident that Li jump diffusion in the monoclinic modification is slower than that in the orthorhombic form. Interestingly, our quantum-chemical calculations show (*vide infra*) that the monoclinic modification is found to be more stable than the orthorhombic one which reveals rapid Li exchange among the three regularly occupied crystallographic positions (in particular, see Fig. 2 in ref. 23).

Table 2 Calculated domain sizes for monoclinic Li_3VF_6 prepared at different temperatures. The values listed were calculated with LaB_6 as standard. The respective precursors were synthesized in different solvents

	Decomposition temperatures and corresponding domain sizes		
	400 °C	500 °C	600 °C
Li_3VF_6, precursor synthesized in THF	37 nm	107 nm	127 nm
Li_3VF_6, precursor synthesized in Et_2O	33 nm	84 nm	160 nm
Li_3VF_6, precursor synthesized in EtOH	44 nm	80 nm	155 nm

Li_3MF_6 (M = Cr, Fe, Co) and Li_2MnF_5

The preparation of the corresponding compounds containing chromium, iron, and manganese was performed in analogy to that of Li_3VF_6. Unfortunately, and in contrast to Li_3VF_6, which can be synthesized with high yields, the designated products could not be prepared as single-phase powders. During the synthesis of the precursor, the formation of larger quantities of the corresponding difluorides occurs. For the preparation of a Li_3FeF_6-precursor, $Fe(acac)_3$ and $Fe(OEt)_3$ were tested in

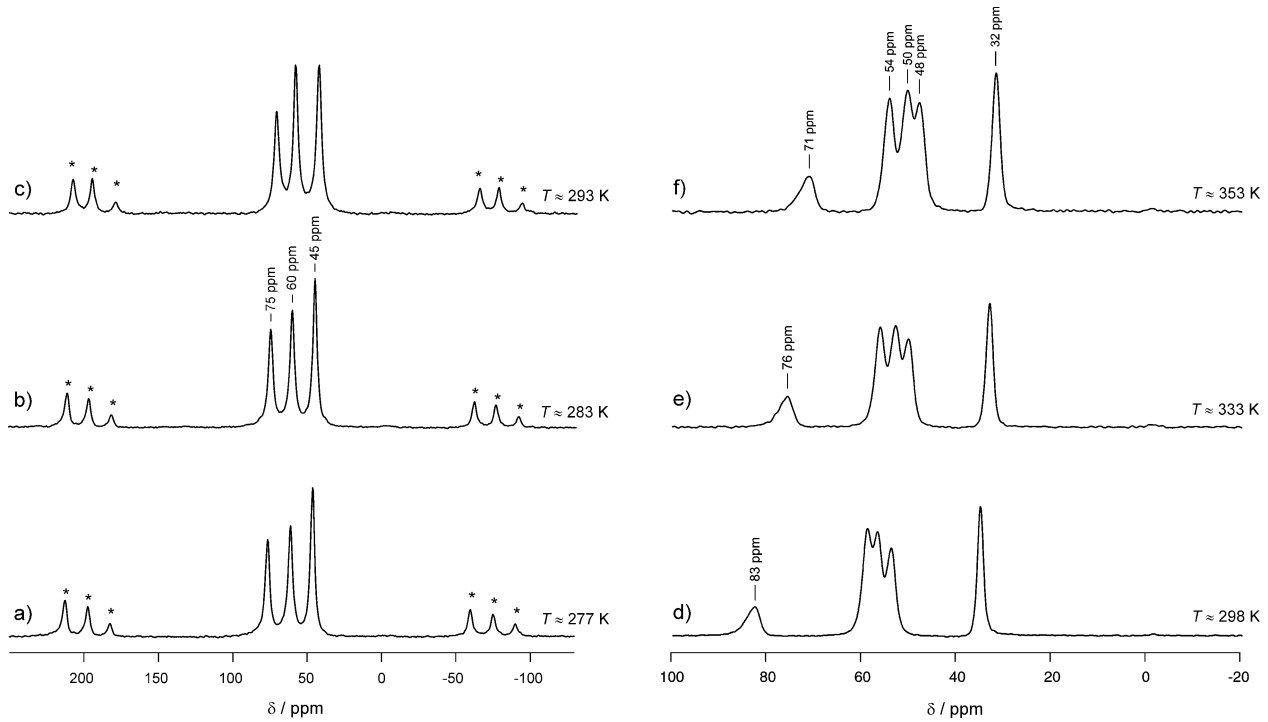

Fig. 4 ^{6}Li MAS NMR spectra of α-Li_3VF_6 (a–c), 12 kHz spinning speed and β-Li_3VF_6 (d–f), 30 kHz spinning speed recorded at the temperatures indicated. Spectra have been referenced to aqueous LiCl. Note that in each case the number of NMR signals detected is in agreement with the crystallographic data of the two polymorphs. The temperature dependence of the NMR shifts points to Curie–Weiss behaviour as expected.

different solvents. Tempering of the obtained orange powder at 400 °C always resulted in a mixture of monoclinic Li_3FeF_6 as well as LiF and FeF_2. The orthorhombic modification of Li_3FeF_6 was also obtained with only a 50% yield. In the case of M = Cr, monoclinic Li_3CrF_6 could be obtained with approximately 85% purity. The precursor was prepared from Li*O*t*Bu, $Cr(acac)_3$ and a HF–EtOH solution (see Fig. 5). Unfortunately, by using Li*O*t*Bu/$Co(acac)_3$/HF, Co^{3+} was completely reduced to Co^{2+} and only LiF and CoF_2 were formed. Surprisingly, in the system Li–Mn–F the formation of Li_2MnF_5 was observed. $Mn(acac)_3$ and $Mn(OAc)_3\cdot 2H_2O$ were used as starting materials. MnF_2 was already formed during the synthesis of the precursor. The variation of the reaction time to prepare the precursor turned out to have no effect on the amount of MnF_2 formed. Interestingly, Li_2MnF_5 with a maximum yield of 30% was only formed by decomposing the precursor synthesized from $Mn(OAc)_3\cdot 2H_2O$ (Fig. 6). Precursors synthesized from $Mn(acac)_3$ yielded only MnF_2 and LiF after decomposition. Compared to conventional solid-state routes reported in the literature, which require temperatures ranging from 700 to 800 °C,[27] the two-step synthesis route followed here allows the preparation of Li_2MnF_5 at temperatures as low as 400 °C.

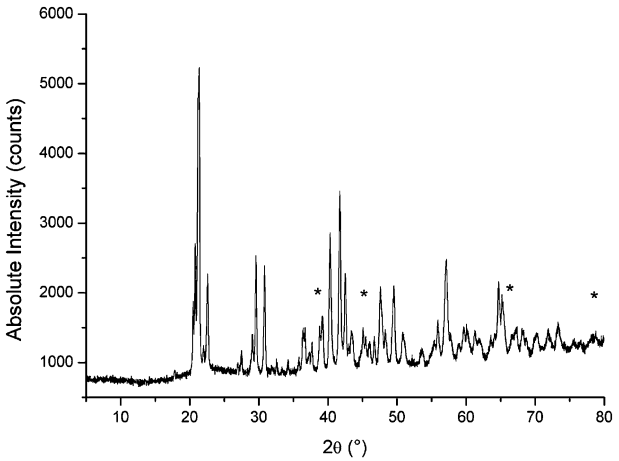

Fig. 5 X-ray powder diffraction pattern of monoclinic Li_3CrF_6 prepared at 500 °C. The sample was slowly cooled down to room temperature (* = LiF).

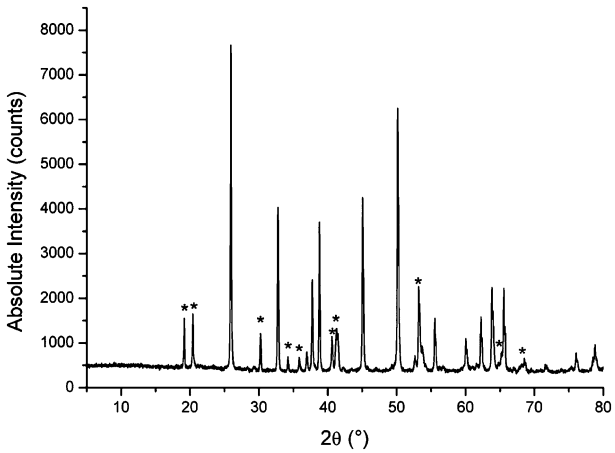

Fig. 6 X-ray powder pattern of Li_2MnF_5 (*). The sample was prepared at 400 °C from $Mn(OAc)_3\cdot 2H_2O$. Other products found are LiF and MnF_2.

Note that the procedure described in ref. 27 is useful to prepare single crystals. However, no information on the yields is given by the authors although preliminary experiments carried out by our group resulted in a maximum yield of 95% when a stoichiometric mixture of LiF and MnF_3 was used in a solid state route (60 h, 480 °C, monel capsule) to obtain Li_2MnF_5.

Preliminary ^{7}Li MAS NMR spectra of Li_2MnF_5, synthesised *via* the above-mentioned solid state route (95% yield), recorded at spinning speeds ranging from 15 to 35 kHz (ambient bearing gas temperature) comprise rather broad resonance lines. The MAS NMR spectrum recorded at 15 kHz (see Fig. 7) reveals an intense line (A) at approximately 180 ppm and another one of lower intensity (B) at 0 ppm (the dashed line is to guide the eye), both with spinning sidebands. The intense line spreads over a range of some hundreds of ppm. The isotropic resonance can be distinguished from the spinning sidebands by recording MAS spectra at different rotation frequencies (see Fig. 7b). As can be clearly seen in Fig. 7b, the heat development, which increases with increasing spinning speed when ambient bearing gas pressure is used, is directly reflected by the shift of the isotropic resonance. As an example, using room temperature bearing gas the isotropic resonance of the main signal shows up at 172 ppm. Reducing the spinning speed by 5 kHz shifts the line towards positive ppm values. Additional heating of the bearing gas causes the line to show up at 162 ppm, as expected.

Thus, the main line clearly reveals a temperature-dependent NMR shift (see the corresponding MAS NMR spectra labeled (ii) and (iii) in Fig. 7b); the associated spin–lattice relaxation time T_1 turns out to be of the order of 2 ms only. This is in contrast to

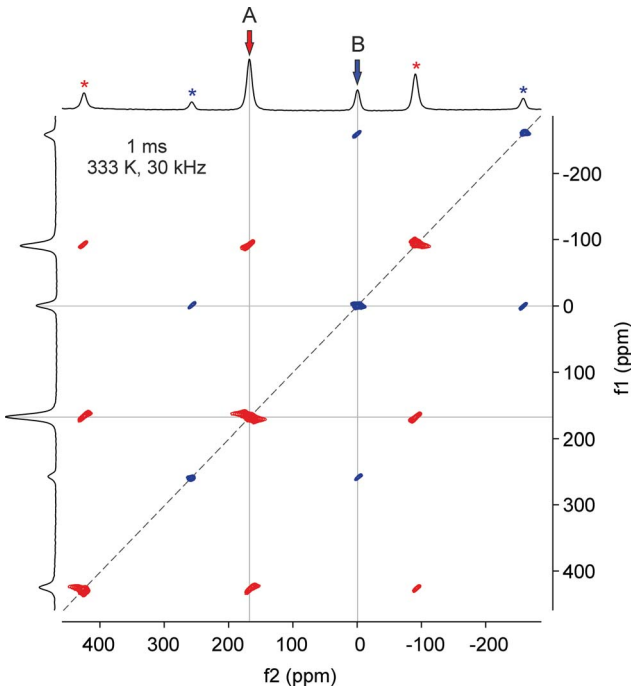

Fig. 8 2D ^{7}Li exchange MAS NMR spectrum (116 MHz) of polycrystalline Li_2MnF_5 recorded at a spinning speed of 30 kHz and heated bearing gas pressure. The mixing time (1 ms) was chosen to be as large as possible; note that the corresponding NMR spin–lattice relaxation time of the main component (A) is approximately 2 ms. No off-diagonal intensities show up in the areas where the solid lines do cross. The dashed line simply connects the diagonal intensities.

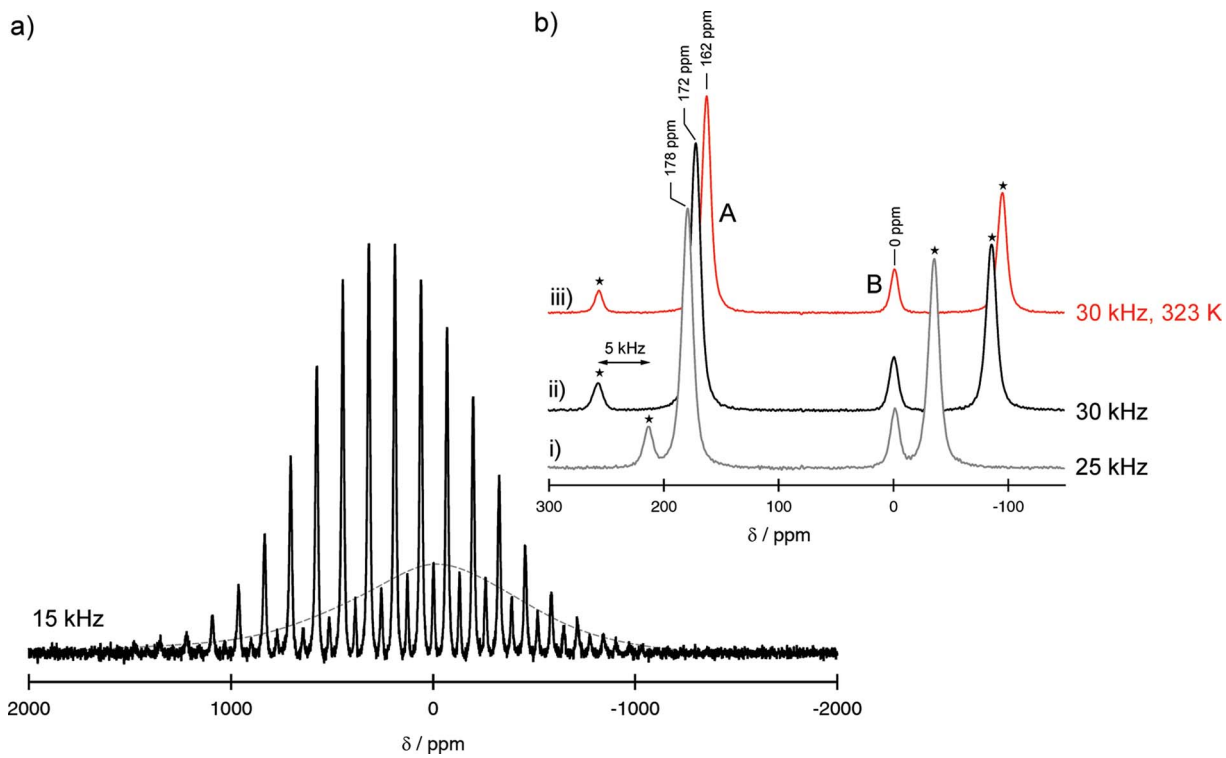

Fig. 7 ^{7}Li MAS NMR spectra of Li_2MnF_5 recorded at (a) 15 kHz spinning speed and (b) at 25 and 35 kHz, respectively. The resonance frequency used was 116 MHz. Except for the spectrum labeled with (iii) ambient bearing gas temperature has been used. The dashed line is to guide the eye. Spinning sidebands, clearly shifting with rotation frequency, are marked with stars.

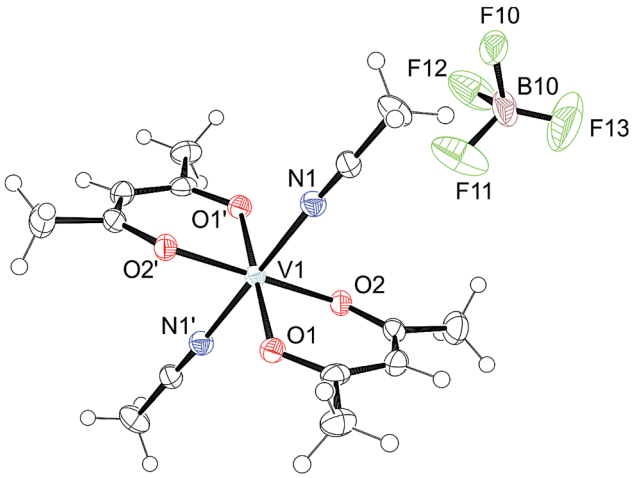

Fig. 9 Crystal structure of $[V(acac)_2(CH_3CN)_2]BF_4$ as derived from X-ray diffraction (ORTEP representation with 50% probability ellipsoids).[37,38]

the line at 0 ppm which is characterized by $T_1 = 1.9$ s. Furthermore, no temperature dependence of this minor NMR component could be observed as shown in Fig. 7b. These findings indicate that the two spin ensembles seem to be magnetically decoupled.

This is supported by the observation that no cross-peaks show up between the isotropic resonances in a 2D exchange MAS NMR experiment (see the signals labeled A and B in Fig. 8), which was carried out at 116 MHz, with a heated bearing gas temperature of 333 K and a mixing time of 1 ms. Off-diagonal intensities are expected to be caused by, *e.g.*, chemical exchange or spin-diffusion between Li sites in the same lattice. The absence of any cross-peaks might indicate that the two signals simply stem from two different phases present whereby the signal at 0 ppm might reflect a (diamagnetic) impurity formed during synthesis (see above) and/or NMR sample preparation, see also ref. 28. In conclusion, at least at ambient temperature and above, the 1D MAS NMR spectra of Li_2MnF_5 reveal a single resonance. This is in good agreement with the crystal structure reported for Li_2MnF_5 showing only one Li site. Further measurements, which are intended to be performed at much lower temperatures, might help in finding out whether the main resonance detected is a coalesced one being the result of fast Li exchange processes between magnetically slightly differing Li positions. Previously, this was reported for Li intercalated $Cr_2Ti_3Se_8$ studied by Wontcheu *et al.*[28]

Crystal structure determination of the Li_3VF_6 precursor

As already described above, X-ray powder diffraction gave no satisfying information on the crystal structure and the species the Li_3VF_6 precursor is composed of. Therefore, further analyses were performed to collect information on the vanadium species and to answer the question of whether Li_3VF_6 is already formed during the synthesis of the precursor or is generated during the annealing step. Such information helps optimize the synthesis conditions of the related precursors used to prepare Li_3FeF_6 and Li_2MnF_5, for example. The Li_3VF_6 precursor described above was complementarily investigated by NMR and FTIR spectroscopy. ^1H and ^{13}C NMR spectra of the removed solvents clearly show the signal of acetylacetone which indicates that acetylacetonate was abstracted. Samples of the Li_3VF_6 precursor were measured in MeOH-d_4 and D_2O, respectively. ^1H NMR signals of acetylacetonate bonded to V^{3+} were observed at 44 ppm. The NMR signals are very broad and have a pronounced low-field shift which is caused by the V^{3+} ion (*vide infra*). The chemical shift corresponds to the values known for $V(acac)_3$.[29,30] The ^{19}F NMR spectra reveal intensities in the range from −124 ppm up to −145 ppm (D_2O). When the samples have been solved in MeOD-d_4 NMR signals at −132 and at −154 ppm show up. NMR lines with chemical shifts ranging from −124 to −135 ppm can be ascribed to Li_2SiF_6.[31] Note that the ^{19}F NMR shifts of $[SiF_6]^{2-}$ depend on the pH-value.[32] Because of exchange reactions they shift to lower fields with increasing pH-value. In the ^{51}V NMR spectra signals at −657 and −896 ppm were observed. The ^{51}V shift for $V(acac)_3$ in MeOD-d_4 shows up at −899 ppm.

FTIR experiments were carried out in transmission mode (50 to 4000 cm^{-1}) and by using an ATR-module (400 to 4000 cm^{-1}, attenuated total reflectance mode). We used samples which were prepared as KBr and CsI pellets. First, let us discuss the far IR range (50 to 400 cm^{-1}). The transmission spectrum shows one band at 295 cm^{-1} which is in good agreement with the ν_4-band of $[VF_6]^{3-}$.[33] Further bands are visible in the organic fingerprint range.[34] The C═O– and C═C combination modes of acetylacetonate appear at 933, 1532 and 1586 cm^{-1}. Further bands can be found at 1033 cm^{-1} ($\rho_r(CH_3)$), 1366 + 1388 cm^{-1} ($\delta_s(CH_3)$) and at 1290 cm^{-1} ($\nu(C–CH_3)$ + $\nu(C:::C)$). Depending on the preparation conditions of the sample, the IR spectra show a broad band in the range from 714 to 741 cm^{-1} which agrees with the ν_3-band of $[SiF_6]^{2-}$.[35] In summary, it might be concluded that the Li_3VF_6-precursor contains several vanadium species including acetylacetonate as well as $[VF_6]^{3-}$.

In addition to the spectroscopic analyses, attempts were made to prepare single crystals. Saturated solutions of the precursor in CH_3CN or MeOH were filled into small glass tubes. These glass

Table 3 Crystal data of $[V(acac)_2(CH_3CN)_2]BF_4$

Chemical formula	$C_{14}H_{20}BF_4N_2O_4V$
Formula mass	418.07
Crystal system	Monoclinic
a/Å	11.9556(10)
b/Å	5.7003(4)
c/Å	15.8568(19)
α/°	90.00
β/°	119.774(7)
γ/°	90.00
Unit cell volume/Å^3	937.99(17)
Temperature/K	150(2)
Space group	$P2_1/c$
Number of formula units per unit cell, Z	2
Radiation type	MoKα
Number of reflections measured	3866
Number of reflections observed	1372
R_σ	0.0635
Number of independent reflections	1832
R_{int}	0.0390
Final R_1 values ($I > 2\sigma(I)$)	0.0450
Final $wR(F^2)$ values ($I > 2\sigma(I)$)	0.1044
Final R_1 values (all data)	0.0633
Final $wR(F^2)$ values (all data)	0.1093

Table 4 Calculated lattice parameters *a*, *b*, *c*, *β* and de-lithiation energy E_d of the compounds Li_3MF_6 and Li_2MnF_5 (method PW1PW). Values in parentheses correspond to measured lattice parameters (orth. = orthorhombic, mon. = monoclinic)

Compound	*a*/Å	*b*/Å	*c*/Å	*β*/°	E_d/eV
Li_3VF_6, orth.	9.53 (9.59)	8.45 (8.49)	5.03 (5.04)		
Li_3VF_6, mon.	14.30 (14.39)	8.68 (8.69)	10.05 (10.06)	96.4 (95.9)	4.73
Li_3FeF_6, orth.	9.58 (9.53)	8.43 (8.24)	5.01 (4.88)		
Li_3FeF_6, mon.	14.34 (14.41)	8.64 (8.67)	10.02 (10.05)	95.6 (95.3)	6.69
Li_3CrF_6, mon.	14.32 (14.43)	8.59 (8.61)	10.02 (10.04)	94.9 (94.6)	6.18
Li_2MnF_5	10.02 (10.02)	4.97 (4.95)	7.39 (7.41)	112.4 (112.2)	5.88

tubes were placed inside a Schlenk tube filled with Et_2O or pentane. From the CH_3CN solutions, dark red crystals of the compound $[V(acac)_2(CH_3CN)_2]BF_4$ were obtained (Fig. 9). This compound shows the existence of acac-containing vanadium species in the precursor. The current work of our group indicates that the here-presented species is just the first one in a sequence of more and more fluorinated species. More details will be given in a forthcoming contribution.[36] BF_4^- is formed by the reaction of HF with the borosilicate glassware during the synthesis of the precursor. V^{3+} is coordinated octahedrally by two acetylacetonate ions and two molecules of CH_3CN. The BF_4^- ion is severely disordered over a center of inversion. Crystal data for $[V(acac)_2(CH_3CN)_2]BF_4$ are given in Table 3.

Quantum-chemical calculations

In order to investigate the suitability of the synthesized Li_3MF_6 compounds as potential cathode materials in lithium-ion batteries, we calculated the corresponding de-lithiation energies at density-functional theory (DFT) level. Based on our experience with open-shell transition metal systems[39] we chose the DFT/Hartree–Fock hybrid functional PW1PW.[40] The calculations were performed with the crystalline-orbital program package CRYSTAL09.[41] The standard atomic basis sets for the elements Li, O, V, Cr, Mn and Fe were taken from the CRYSTAL homepage[42] and augmented where possible with diffuse shells and polarization functions. A detailed description of the optimized solid-state basis sets will be given elsewhere.[43] The computational accuracy parameters were set to rather strict values as described previously.[39] In Table 4 the calculated lattice parameters are compared with our measured values obtained from X-ray powder diffraction where available (*vide supra*). The agreement found between theory and experiment for the structure parameters is encouragingly good. In all cases the deviations are below 1% except the *b* and *c* lattice vectors of orthorhombic Li_3FeF_6. This indicates that our theoretical approach is sufficiently accurate to describe the transition metal fluorides. For Li_3VF_6 and Li_3FeF_6 we computed the relative stability of the orthorhombic and monoclinic phases. In both cases the monoclinic polymorph was more stable so that only this phase was considered for the calculation of the de-lithiation energy E_d. For all compounds we also investigated the magnetic structure. Ferromagnetic and antiferromagnetic couplings were considered. For example, for Li_2MnF_5 the previously reported antiferromagnetic chains of Mn^{3+} ions were considered.[44]

The de-lithiation energy was computed by removing all Li atoms occupying a certain Wyckoff position. As discussed above there are five crystallographically inequivalent Li atoms in the asymmetric unit of monoclinic Li_3MF_6. In Li_2MnF_5 the two Li atoms of the primitive unit cell are crystallographically equivalent. In the antiferromagnetic ground state they are not electronically equivalent anymore. However, the differences between local electrostatic potentials and electric field gradients are rather small. In Table 3 we only report the smallest values of the de-lithiation energies for each compound according to the following equation:

$$Li_{3n}M_nF_{6n}(s) = xLi(s) + Li_{3n-x}M_nF_{6n(s)}$$

with lithium metal as reference according to the electrochemical reference. *x* corresponds to the number of Li ions occupying the particular Wyckoff position. E_d is then normalized to one Li atom. Since only one electron is transferred in this process, E_d in eV directly corresponds to a battery voltage in V (for approximations see below). It has to be noted that in the present lithium-ion batteries graphite is used as the counter anode rather than metallic lithium, but the potential differences are rather small. The present values can only be regarded as zero-order approximations since we did not take into account possible phase transitions after Li removal. The change in Li concentration is rather large in our models due to the small unit cell size. This means that we calculate an average value of the potential for the corresponding *x* range rather than $E_d(x)$ as in electrochemical measurements. Furthermore, enthalpy and entropy are not taken into account due to the high computational effort. Nevertheless, we have shown in a parallel study that the simplistic approach described here can indeed reproduce measured cell potentials of a wide range of battery materials with surprisingly high accuracy.[45] The resulting E_d values presented in Table 3 may therefore have some significance. As they range from 4.7 to 6.7 eV, not too far from the initially discussed theoretical result (6 eV) for $LiCaCoF_6$ or $LiCdCoF_6$,[8] all materials synthesized in this work can be regarded as promising high-voltage cathode materials provided that stability issues are resolved.

Conclusions

Ternary lithium fluorides of transition metals were synthesized *via* a sol–gel route from transition metal acetylacetonates as precursors and hydrogen fluoride in organic solvents. The two polymorphs of Li_3VF_6 were obtained with approximately 98% purity. Local environments probed by high-resolution solid-state ^6Li and ^7Li NMR are in very good agreement with expectations from the crystal structure of the compounds. The synthesis of the monoclinic phase is already possible at temperatures as low as 300 °C. Its domain size can be controlled by modifying the temperature used for the synthesis. This may be of importance in

the preparation of cathode materials for lithium-ion batteries. Monoclinic Li_3CrF_6 was also prepared with a phase purity of approximately 85%. For manganese, iron and cobalt the corresponding difluorides were formed in addition to the ternary fluorides. Quantum chemical calculations show that all materials have high de-lithiation energies making them suitable candidates to be used as high-voltage battery cathode materials.

Acknowledgements

We thank the German Ministry of Education and Research (BMBF) for financial support within the LIB 2015 initiative, project HE-Lion. We thank D. Freude and E. Romanova (Leipzig) for recording of some of the NMR measurements presented. M.W. gratefully acknowledges financial support by the Deutsche Forschungsgemeinschaft (DFG). We would also like to thank Mr Manfred Detlaff (NMR service group, TU Berlin) and Ms Paula Nixdorf (XRD service group, TU Berlin) for their experimental help.

Notes and references

1 J. M. Tarascon and M. Armand, *Nature*, 2001, **414**, 359.
2 L. F. Nazar, G. Goward, F. Leroux, M. Duncan, H. Huang, T. Kerr and J. Gaubicher, *Int. J. Inorg. Mater.*, 2001, **3**, 191.
3 M. S. Whittingham, *Chem. Rev.*, 2004, **104**, 4271.
4 A. S. Aricó, P. Bruce, B. Scrosati, J.-M. Tarascon and W. V. Schalkwijc, *Nat. Mater.*, 2005, **4**, 366.
5 P. G. Bruce, B. Scrosati and J.-M. Tarascon, *Angew. Chem., Int. Ed.*, 2008, **47**, 2930.
6 B. L. Ellis, K. T. Lee and L. F. Nazar, *Chem. Mater.*, 2010, **22**, 691–714.
7 J. B. Goodenough and Y. Kim, *Chem. Mater.*, 2010, **22**, 587.
8 Y. Koyama, I. Tanaka and H. Adachi, *J. Electrochem. Soc.*, 2000, **147**, 3633.
9 E. Gonzalo, A. Kuhn and F. Garcia-Alvarado, *J. Power Sources*, 2010, **195**, 4990–4996.
10 (*a*) I. Gocheva, K. Chihara, S. Okada and J. Yamaki, *Lithium Batteries Discussion 2011 – Electrode Materials – Archacon, France (extended abstract)*; (*b*) A. Basa, E. Gonzalo, A. Kuhn and F. Garcia-Alvarado, *J. Power Sources*, 2012, **207**, 160–165.
11 W. Massa, *Z. Kristallogr.*, 1980, **153**, 201–210.
12 W. Massa and W. Ruedorff, *Z. Naturforsch., B*, 1971, **26**, 1216–1218.
13 P. Heitjans and S. Indris, *J. Mater. Sci.*, 2004, **39**, 5091–5096.
14 M. Wilkening, V. Epp, A. Feldhoff and P. Heitjans, *J. Phys. Chem. C*, 2008, **112**, 9291.
15 P. Heitjans, M. Masoud, A. Feldhoff and M. Wilkening, *Faraday Discuss.*, 2007, **134**, 67.
16 E. Avvakumov, M. Senna and N. Kosova, *Soft Mechanochemical Synthesis: A Basis for New Chemical Technologies*, Kluwer Academic Publishers, Boston, 2001.
17 K. L. Da Silva, D. Menzel, A. Feldhoff, C. Kübel, M. Bruns, A. Paesano, A. Düvel, M. Wilkening, M. Ghafari, H. Hahn, F. J. Litterst, P. Heitjans, K. D. Becker and V. Šepelák, *J. Phys. Chem. C*, 2011, **115**, 7209–7217.
18 A. Düvel, M. Wilkening, R. Uecker, S. Wegner, V. Šepelák and P. Heitjans, *Phys. Chem. Chem. Phys.*, 2010, **12**, 11251–11262.
19 E. Kemnitz, U. Groß, S. Rüdiger and C. S. Shekar, *Angew. Chem.*, 2003, **115**, 4383–4386.
20 St. Wuttke, A. Vimont, J.-C. Lavaley, M. Daturi and E. Kemnitz, *J. Phys. Chem. C*, 2010, **114**, 5113–5120.
21 M. Ahrens, G. Scholz, M. Feist and E. Kemnitz, *Solid State Sci.*, 2006, **8**, 798–806.
22 (*a*) D. L. Deadmore, J. S. Machin and A. W. Allen, *J. Am. Ceram. Soc.*, 1962, **45**, 120–122; (*b*) Yu. N. Moskvich, B. I. Cherkasov and G. I. Dotsenko, *Zh.Strukt. Khim.*, 1979, **20**, 348–357.
23 M. Wilkening, E. Romanova, S. Nakhal, D. Weber, M. Lerch and P. Heitjans, *J. Phys. Chem. C*, 2010, **114**, 19083.
24 T. L. Spencer, A. Ramzy, V. Thangadurai and G. R. Goward, *Chem. Mater.*, 2011, **23**, 3105–3113.
25 P. Bottke, S. Nakhal, M. Lerch, M. Wilkening and P. Heitjans, *Diff. Fundam.*, 2011, **16**, 40.
26 T. Ressler, *WINXAS v3.1* 2011.
27 J. Pebler, W. Massa, H. Lass and B. Ziegler, *J. Solid State Chem.*, 1987, **71**, 87–94.
28 J. Wontcheu, W. Bensch, M. Wilkening, P. Heitjans, S. Indris, P. Sideris and C. P. Grey, *J. Am. Chem. Soc.*, 2008, **130**, 288.
29 A. Johnson and G. W. Everett, *J. Am. Chem. Soc.*, 1972, **94**, 1419–1425.
30 D. R. Eaton, *J. Am. Chem. Soc.*, 1965, **87**, 3087–3102.
31 P. M. Borodin and N. Kim Zao, *Russ. J. Inorg. Chem.*, 1972, **16**, 1720–1722.
32 W. F. Finnery, E. Wilson, A. Callender, M. D. Morris and L. W. Beck, *Environ. Sci. Technol.*, 2006, **40**, 2572–2577.
33 R. Becker and W. Sawodny, *Z. Naturforsch.*, 1973, **28b**, 360.
34 M. Mikami, I. Nakagawa and T. Shiraanouchi, *Spectrochim. Acta*, 1967, **23A**, 1037.
35 C. Naulin and R. Bougon, *J. Chem. Phys.*, 1976, **64**, 4155.
36 J. Kohl, D. Wiedemann, S. Troyanov and M. Lerch, in preparation.
37 Crystal data for $[V(acac)_2(CH_3CN)_2]BF_4$ were collected on an Oxford Diffraction Xcalibur S diffractometer equipped with an Enhance Mo-K_α source (graphite monochromated, $\lambda = 0.71073$ Å) and a Sapphire 3 detector at $T = 150$ K. The structure was solved with SHELXS-97 and refined against all F^2 data using the full-matrix least-squares method of SHELXL-97. The tetrafluoroborate moiety is disordered over an inversion centre. The positional disorder was not further resolved resulting in somewhat higher displacement parameters.†
38 G. M. Sheldrick, *Acta Crystallogr., Sect. A: Found. Crystallogr.*, 2008, **64**, 112–122.
39 M. M. Islam, T. Bredow and A. Gerson, *ChemPhysChem*, 2011, **12**, 3467–3473.
40 T. Bredow and A. R. Gerson, *Phys. Rev. B: Condens. Matter*, 2000, **61**, 5194–5201.
41 R. Dovesi, R. Orlando, B. Civalleri, C. Roetti, V. R. Saunders and C. M. Zicovich-Wilson, *Z. Kristallogr.*, 2005, **220**, 571–573.
42 http://www.crystal.unito.it/Basis_Sets.
43 N. Ferro, C. Reimann and T. Bredow, in preparation.
44 T. Roisnel, P. Nuñez, W. Massa and A. Tressaud, *Phys. B*, 1997, **234–236**, 579–581.
45 N. Ferro, M. Lerch, R. Glaum, H. Ehrenberg and T. Bredow, in preparation.